



Extracting region-specific runout behavior and rainfall thresholds for massive landslides using seismic records: a case study in southern Taiwan

Ching Hung¹ · Guan-Wei Lin² · Ben Leshchinsky³ · Hsien-Li Kuo²

Received: 6 May 2018 / Accepted: 5 September 2018 / Published online: 13 September 2018
© Springer-Verlag GmbH Germany, part of Springer Nature 2018

Abstract

Typhoon Morakot struck Taiwan on 7 August 2009, bringing severe rainfall and landslides. Of the many landslides caused by the storm, 12 large-scale landslides were discovered based on seismic signals recorded from broadband seismic stations. Landslides inventoried from both seismic records and satellite imagery are used as baseline data to evaluate region-specific forensic analyses of landslide features, e.g. disturbed area, width and runout distance (D_{runout}), associated with landslide-induced seismic signals and signal durations (Δt). The results of these analyses show that (i) the landslide-disturbed area correlated well with signal duration when Δt was over 60 s; (ii) the landslide-disturbed area correlated well with the ratio of the landslide width to runout distance when Δt was under 40 s; (iii) the runout distance of sliding mass exhibited a positive relation with Δt^2 , satisfying the energy conserved during mass movement. This case study presents a region-specific examination of the Δt - D_{runout} relationship based on 12 large-scale landslides that occurred during Typhoon Morakot, providing insight into the sliding processes. In addition, the time of landslide initiation was extracted from seismic signals in order to better understand region-specific, large-scale, landslide rainfall thresholds. These relationships indicate that (a) long-duration rainstorms with high cumulative rainfall tend to dictate the occurrence of large-scale landslides; (b) the rainfall threshold for large-scale landslides is found to be higher than in previous studies that also include smaller landslides, defined in this region as $I = 60D^{-0.31}$, where I is the rainfall intensity (mm/h) and D is the duration (h) of the rainstorm.

Keywords Large-scale landslide · Ground-motion · Runout distance · Landslide initiation time · Rainfall threshold

Introduction

Typhoon Morakot struck Taiwan during August 7–10 2009, bringing severe rainfall and flooding to much of the southern part of the country. As a result, cumulative rainfall in excess of 2000 mm, with a maximum 24-h rainfall of over 1000 mm (CWB 2013) was recorded, resulting in the occurrence of

more than 20,000 landslides and debris flows in southern Taiwan (Lin et al. 2011; Tsou et al. 2011; Wu et al. 2011; Kuo et al. 2013). These landslides caused considerable damage to roads, bridges, and other critical infrastructure, hindering emergency and recovery efforts resulting from the large storm. Accordingly, there has been significant effort into better defining region-specific rainfall thresholds for landslide hazard assessment.

To better evaluate landslide hazards stemming from extreme precipitation events, it is essential to understand the conditions that cause failure and the movement of debris following rupture (Cruden and Varnes 1996; Chen et al. 2013; Ekstrom and Stark 2013; Lin et al. 2017; Hung et al. 2017, 2018). In particular, accurate assessment of landslide initiation time, location, and size are beneficial for understanding when and how slopes may fail following precipitation. Remote sensing techniques, such as lidar, satellite imagery, and radar are of particular use for

✉ Guan-Wei Lin
gwlin@mail.ncku.edu.tw

¹ Department of Civil Engineering, National Cheng Kung University, No. 1, University Road, Tainan City, Taiwan

² Department of Earth Sciences, National Cheng Kung University, No. 1, University Road, Tainan City, Taiwan

³ Department of Forest Engineering, Resources & Management, Oregon State University, 280 Peavy Hall, Corvallis, OR 97331, USA

estimating the location and debris volumes of landslides, but are often subject to poor temporal resolution (Kimura and Yamaguchi 2000; Nichol and Wong 2005; Jaboyedoff et al. 2012). The gaps in scheduled remotely sensed data collection preclude accurate estimates of landslide failure time; knowledge of such the exact moment of landslide initiation and travel provide context towards potential drivers—e.g. cumulative rainfall, ground accelerations and directionality. However, a combination of high-resolution remote sensing data used for accurate landslide debris estimates *and* use of inferred seismic data to estimate landslide initiation time provides insight into the magnitude, timing, movement, and material properties of large-volume landslides (Kanamori and Given 1982; Kawakatsu 1989; Brodsky et al. 2003; Chen et al. 2014; Hibert et al. 2014). This information may be used to better assess precipitation-induced landslide hazards in context of regional geology and conditions.

During Typhoon Morakot, there were several landslide-induced ground motions recorded by the Broadband Array in Taiwan for Seismology (BATS); some of these records were used to estimate the timing and location of a fatal landslide dam formed during the storm (Lin et al. 2010; Feng 2011; Kao et al. 2012; Feng 2012). In recent years, landslide-induced ground motions have increasingly gained interest as a means of assessing the location, magnitude, and movement processes of landslides (Dammeier et al. 2011; Kao et al. 2012; Chen et al. 2013; Lin et al. 2015; Chao et al. 2016). These techniques better inform our understanding of landslide dynamics and thresholds for triggering and provide more tailored hazard assessment to specific regions or geologies. However, due to the empirical nature that outlines regional evaluation of landslide triggering and runoff dynamics from heavy precipitation, rainfall-landslide relationships are proposed for southern Taiwan based on recorded ground motions resulting from catastrophic landslides that occurred during Typhoon Morakot. These relationships may also provide further insight into the relationship between geomorphic changes and landslide-induced ground motions.

In this case study, the 12 ground motion records resulting from large-scale landslides reported by Chen et al. (2013) are examined to better define relationships into landslide triggering time, precipitation, runoff duration, landslide area, and landslide deposition area. This unique ground motion dataset allows for an opportunity to directly compare seismic information with the geomorphic features to enhance interpretation of precipitation-induced landslide movements. Furthermore, the technical framework for seismic inversion and subsequent evaluation of landslide initiation and termination times are described. Finally, the cumulative rainfall-landslide threshold relationships for large-scale landslides inferred from seismic records are proposed.

Methodology and site description

Site geology and climate

This study focuses on the well-instrumented upstream catchments of the Kaoping River, Linpien River, and Taimali River (Fig. 1). The geology of the catchments varies from sedimentary rock (i.e. mudstone and sandstone), shale in the western sector to metamorphic rocks (i.e. slate and schist), and phyllite in the eastern sector (Ho 1994) (Fig. 2). The average annual rainfall in the area of interest exceeds 3000 mm (Shieh 2000), increasing from the north to the south (Chen et al. 2011). The annual precipitation is primarily concentrated during typhoon season (June–October). It is noted that the observed abundance of rocky soil and colluvium is indicative of frequent landsliding, compounded from not only rainfall, but frequent earthquakes. Due to the seismic nature of the region, there is an extensive network of over 25 high-frequency broadband seismometers covering an area of over 350 km × 400 km to

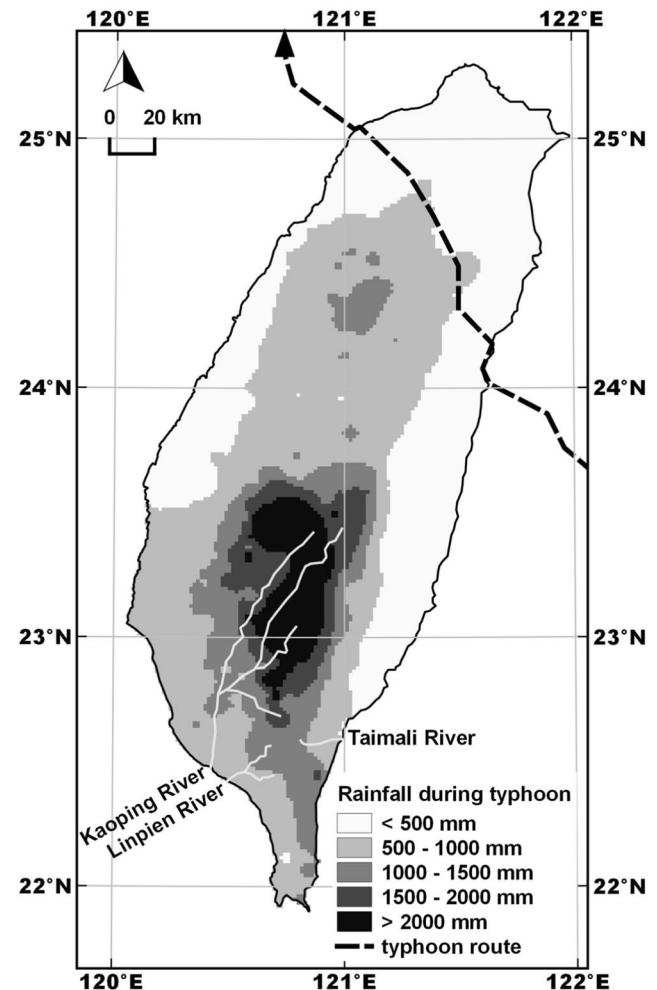


Fig. 1 Distribution of cumulative rainfall during Typhoon Morakot (August 7–10 2009) and the locations of the Kaoping River, the Linpien River, and the Taimali River

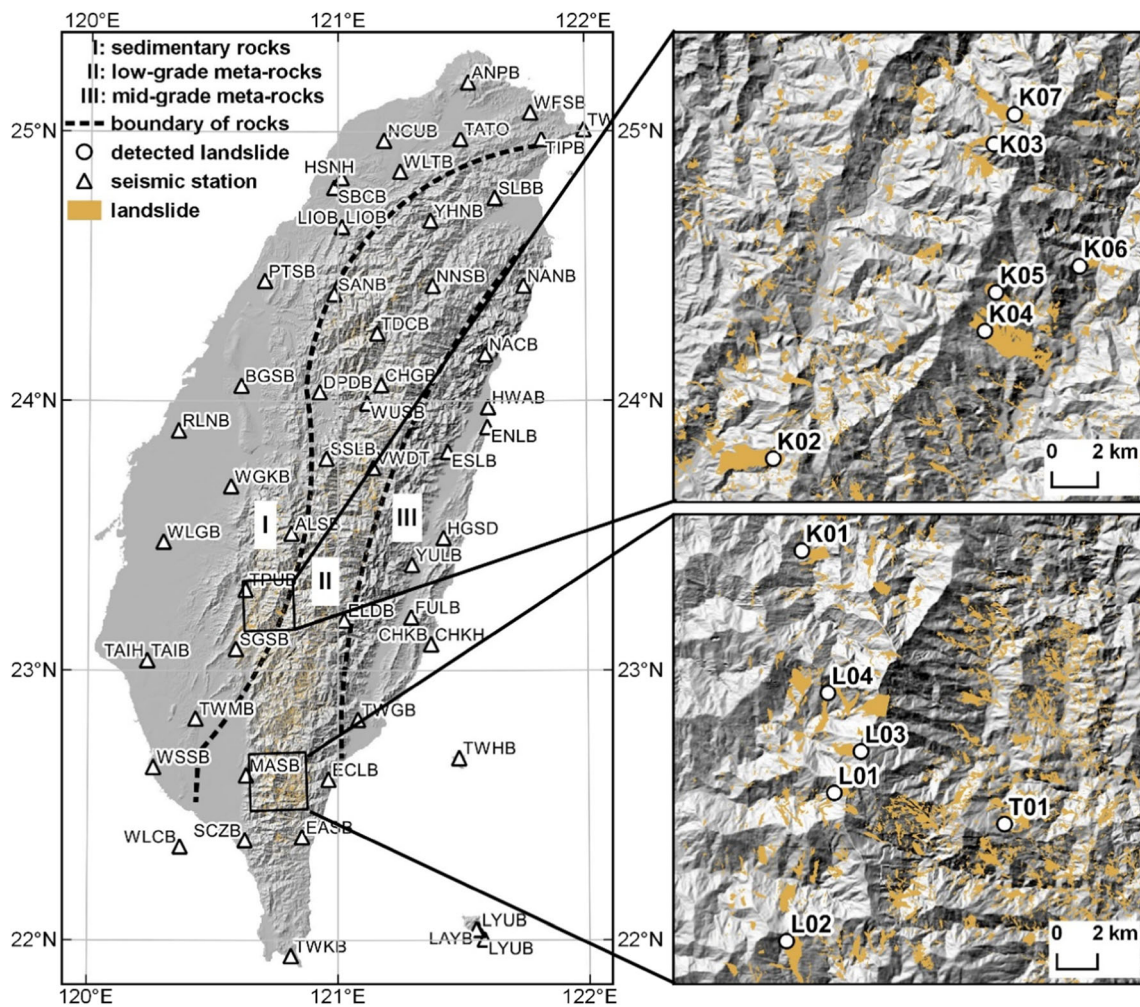


Fig. 2 Distribution of major lithology and seismic station. Brown spots indicate the landslides interpreted through 8-m-resolution satellite imagery. The seismicity-detected landslides were marked in the two right-hand sub-figures

monitor ground motions during earthquakes (IES 1996). These data are used for analysis of landslide duration in this case study.

Typhoon Morakot struck during the period of 5–10 August 2009, with the most severe rainfall occurring in southern Taiwan from 7 to 9 August. At the Mt. Wei-liao rainfall station, the cumulative precipitation for 24- and 48-h durations was 1402 mm and 2146.5 mm, respectively, which are very close to the world records of 1825 mm and 2467 mm (Burt 2007). Moreover, 31 rainfall stations had cumulative precipitation of over 1000 mm in 24 h, and 46 rainfall stations recorded precipitation over a 200-year returned period (CWB 2013). Much of this precipitation was concentrated in southern Taiwan, including the study catchments, causing more than 20,000 landslides. Among these landslides, 484 slides were recognized with an area larger than 0.1 km², classified as a large-scale landslide (Lin et al. 2011). The Shiaolin landslide with an area of 2.5 km² occurred in the Kaoping River catchment, and its induced ground motions were observed from the record of the nearby Chiahsien seismic station (Lin

et al. 2010; Kao et al. 2012). Subsequently, Chen et al. (2013) reported 12 ground motions induced by large-scale landslides occurred during Typhoon Morakot. In this study, these time information of the 12 landslides reported by Chen et al. (2013) were selected to investigate their surface features and compare with the time information extracted from seismic records.

Landslide mapping, timing of failure, and duration

The landslides triggered by typhoon Morakot were first mapped using satellite imagery with 8-m pixel resolution, providing a preliminary landslide inventory validated after prior landslides were removed manually. To prevent misinterpretation, only landslides with a projected area over nine pixels (representing areas larger than 576 m²) were recognized. In addition, in order to exclude landslides that occurred before Typhoon Morakot, images from recognized pre-typhoon landslides are compared with those taken after. Afterwards, the locations of 12 large-scale (i.e. exceeding 0.3 km²), long-runout landslides reported by Chen et al.

(2013) were selected for a strategic assessment of timing of failure and failure duration. These landslides were assigned classifications from L01, T01 to K07 in the chronological order of landslide occurrence. Of the 12 landslides considered in this case study, four landslides (L01–04) were located in the Linpien River basin, seven landslides (K01–07) were located in the Kaoping River basin, and one landslide (T01) was located in the Taimali River basin (Fig. 2). According to regional geologic characterizations performed by the Central Geological Survey of Taiwan (Ho 1994; Central Geological Survey 2013), seven landslides (K01, K02, K03, K04, K05, K06, and K07) overlaid sedimentary strata that are mainly composed of interbedded sandstone and shale, whereas their sliding directions were approximately parallel to the dip direction of bedding. The other five landslides (L01, L02, L03, L04, and T01) overlaid low-grade metamorphic rocks that are mainly composed of slate and phyllite with apparent and dominant weak discontinuities. Therefore, the failure mechanism of these landslides was translational in nature. Table 1 provides a list of the landslides and the values of seismic and geomorphic characteristics. Fig. 3a shows eight geometric elements that were determined through satellite imagery and the digital elevation models (DEMs). The pre- and post-typhoon DEMs with resolution of 20 m were employed to derive DEM differentials, which were used for mapping source areas and deposit areas. For each of the 12 landslides targeted in this study, estimates of source area (A_1), deposit area (A_2), horizontal projection of runout distance (D_{runout}), total disturbed area (A), and the average width of the source area (W), were all interpreted through use of 5 m-resolution aerial photos based on the suggested measurement methods for landslide features

proposed by Cruden and Varnes (1996). The runout distance (D_{runout}) was defined as the length between the centroids of the source area (C_1) and deposit area (C_2). The average width of source area (W) was defined as the length of a line running perpendicular to the runout direction and passing through the centroid of the source area, processed using ArcGIS. The runout distance (D_{runout}) and the slope gradient (θ) were calculated based on the triangulation of the topographic relief and horizontal projection of the runout distance. These geometric parameters associated with landslide morphology and travel are useful when considering assessment of initiation time and runout duration, determined from analysis of seismic records.

Determination of the initiation time and termination time for each of the landslides were determined from an analysis of the landslide-induced seismic signals. A landslide generates seismic signals, including the first clear arrivals of the very-low-frequency signals (< 1 Hz) and the high-frequency signals. The very-low-frequency signals induced by landslides can propagate along distances of more than 2000 km. The high-frequency seismic signals induced by landslides are likely the P-waves propagated through the crust; thus, these waves decayed substantially with distance (Lin 2015). Therefore, the characteristics of landslide-induced signals in the frequency domain appear as a unique triangular time/frequency signature in the 1–5 Hz frequency band. The predominant frequency band of the landslide signals is between 0.02 and 5 Hz. In comparison, the signal energy of a local earthquake exhibits a much wider spectral content with frequencies up to ~50 Hz (Kao et al. 2012). In this case study, the 5-min long spectrograms generated using a wavelet transform are created to display the spectrums of frequencies of seismic signals as they

Table 1 Seismic and geomorphic characteristics of the 12 landslides detected by ground motions

ID	River basin	Date UTC	Time UTC	Location		Δt [s]	A [km ²]	D_v [m]	D_{runout} [m]	θ [degrees]	V [ms ⁻¹]	M_s	μ
				°N	°E								
L01	Linpien	2009/08/08	00:04	22.50	120.71	25	0.37	467	1381	20	55.3	4.6	0.24
L02	Linpien	2009/08/08	17:05	22.49	120.73	80	0.93	884	2652	19	33.1	4.6	0.33
K01	Kaoping	2009/08/08	18:19	22.65	120.73	40	1.44	392	1675	14	41.9	5.1	0.19
L03	Linpien	2009/08/08	20:15	22.57	120.75	35	0.74	1151	1971	36	56.3	4.8	0.62
K02	Kaoping	2009/08/08	22:16	23.16	120.63	100	2.17	718	3231	13	32.3	5.2	0.21
K03	Kaoping	2009/08/08	23:14	23.30	120.73	30	0.62	502	1301	23	43.4	4.4	0.34
K04	Kaoping	2009/08/09	00:34	23.23	120.74	25	1.06	310	1356	20	54.2	4.9	0.12
K05	Kaoping	2009/08/09	02:52	23.24	120.73	30	0.85	632	1518	25	50.6	4.7	0.36
L04	Linpien	2009/08/09	03:55	22.57	120.73	60	0.71	657	2181	18	36.4	4.9	0.28
T01	Tamali	2009/08/09	09:31	22.56	120.82	90	2.28	908	2915	18	32.4	5.4	0.31
K06	Kaoping	2009/08/10	03:54	23.24	120.77	30	0.3	369	1141	19	38.0	4.6	0.27
K07	Kaoping	2009/08/10	04:22	23.32	120.77	80	1.57	811	2392	20	29.9	5.0	0.34

Δt means the duration of landslide movement; A means the landslide-disturbed area; D_v means the altitude difference of landslide mass; D_{runout} represents the runout distance; θ represents the average slope gradient of landslide; M_s represents the calculated surface wave magnitude; μ represents the calculated friction coefficient

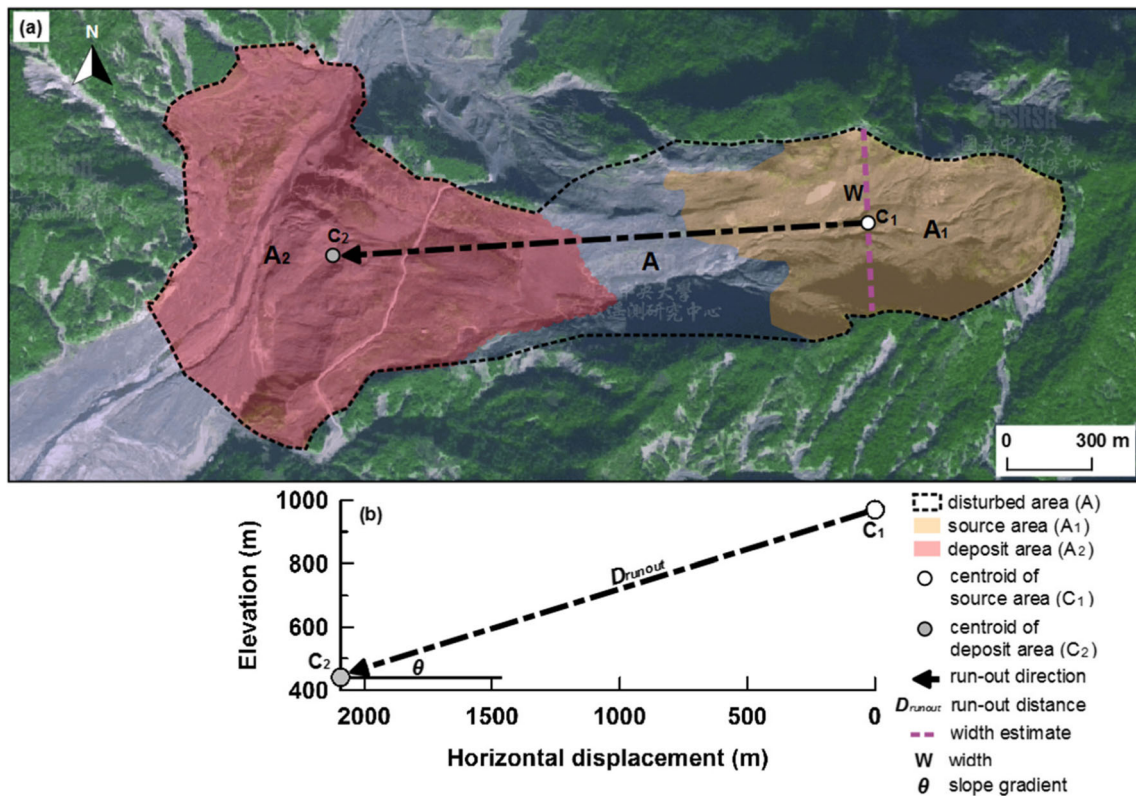


Fig. 3 An example of estimating geometric elements. Runout distance of landslide movement calculated by triangulation with the altitude difference and horizontal projection of runout distance. The open

satellite image is sourced from the Center for Space and Remote Sensing Research, National Central University

vary with time. Then, a landslide detection method, described below, applies pattern recognition to spectrograms attained from recorded ground motions was used. Specifically, analyzed spectrograms inherit a unique triangular time/frequency signature in the 1–5 Hz frequency band (Surinach et al. 2005; Chen et al. 2013) that may be isolated for analysis. This triangular signature is useful for finding landslide-induced ground motions, such as those from Typhoon Morakot (Fig. 4).

Subsequently, to determine the initiation time for the landslide-induced seismic signals, a STA/LTA detection-algorithm, commonly used to detect weak-motion seismic signals, was used in the case study. The STA/LTA algorithm continuously calculates the average values of the absolute amplitude of a seismic signal in two consecutive moving-time windows. The short-time window (STA) is sensitive to seismic events while the long-time window (LTA) provides information about the temporal amplitude of seismic noise at the seismic station. As the ratio of STA to LTA exceeds a preset, triggering threshold, an event is declared. Successful capture of landslide-induced seismic signals depends on proper settings of the detection parameters. These parameters have been tested and proposed by Chen et al. (2013). Based on the detection threshold proposed by Chen et al. (2013), the detection-algorithm implemented in this study employs the ratio of the average signals in 0.5 s to the average signals in 10 s within

the function of the envelope of the horizontal components. A STA/LTA ratio threshold of three is adopted to determine the initiation time (T_1) of landslides (Fig. 4). The termination-time (T_2) of landslides is determined when the amplitude of the function of horizontal envelop descends below 5% of the PGV amplitude for at least five seconds. The time duration between times T_1 and T_2 is defined as the sliding duration (Δt). From this information, the average quasi-front velocity of sliding mass is introduced as a ratio of $D_{runout}/\Delta t$. The velocity, travel duration and travel distance of these landslides is informative for assessing the potential impacts of large, precipitation-induced landslides in southern Taiwan.

Assessment of landslide-rainfall thresholds

Corroborating cumulative precipitation with the initiation time and geomorphic data of the large, precipitation-induced landslides described in this case study provides insight into the thresholds associated with incipient slope failure. The records of rainfall gauges located within the distance of 5 km to the landslide areas were used to investigate the rainfall threshold for large, long-runout landslides in given geology and climate. The characteristics of rainstorm included rainfall duration D (h), cumulative rainfall R (mm), and average intensity I (mm/h). In this study, the beginning of a rainstorm was defined as

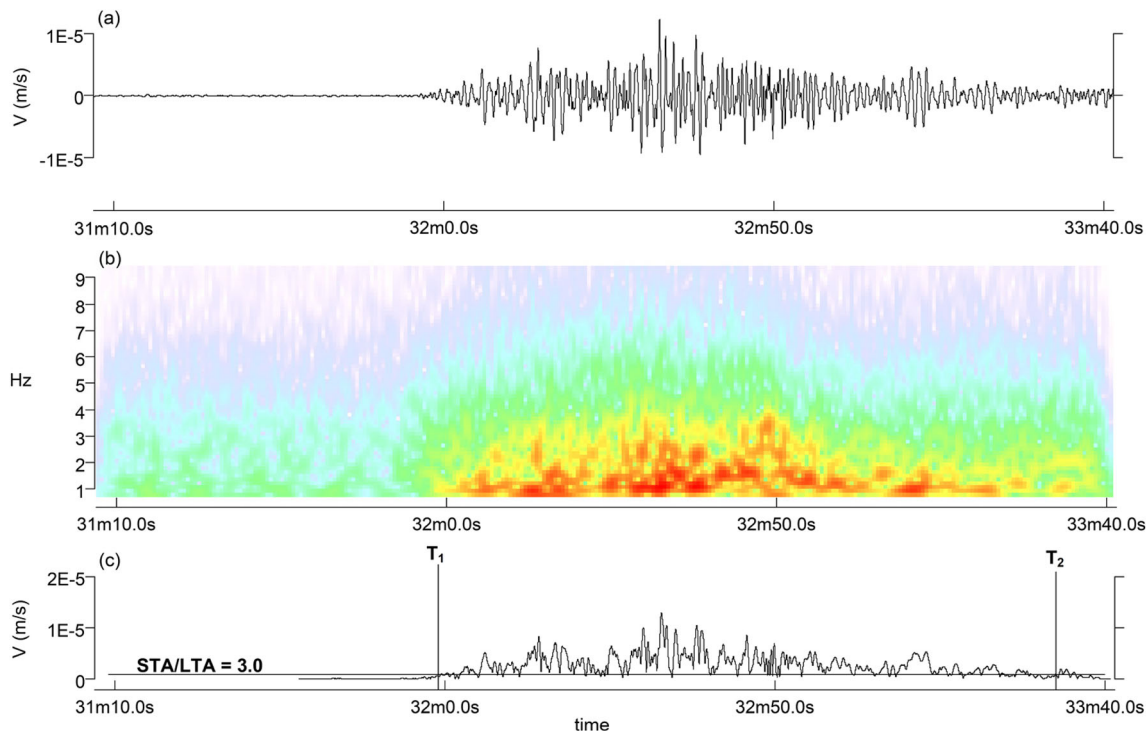


Fig. 4 (a) Original vertical-component velocity records at station MASB. (b) The spectrogram of the T01 landslide at station MASB. (c) Filtered horizontal envelope functions of the T01 landslide at station MASB

the time when rainfall intensity exceeds 4 mm/h. The critical rainfall associated with landsliding was defined as the precipitation accumulated from the beginning of typhoon to the initiation time of slope failure, determined from recognition of seismic patterns described above.

Results and discussion

Landslide-induced ground motions and geomorphic features

The areas of the observed landslides ranged from 0.3 km² to 2.28 km². According to the results, landslides T01 and K02 have the largest disturbed areas, in excess of 2 km², where the significant volume of debris created natural dams, blocking downstream channels. The runout distances of both events exceeded 1300 m; the K02 landslide had the longest runout distance of 3231 m. Tragically, the debris from the K02 landslide covered the downslope village, resulting in significant casualties. For the analyzed set of slides, the observable ground motions triggered by runout did not exceed 2 min; rather, it ranged between 25 to 100 s. It was found that the K02 landslide possessed both the longest duration and runout distance.

Since the estimated average runout velocities of the 12 events all exceeded 5 m/s, all of the events are classified as extremely rapid landslides (Varnes 1978; Cruden and Varnes

1996). The five landslides in the Linpien River basin and the Taimali River basin had average velocities ranging from 32.4 m/s to 56.3 m/s, while the seven landslides in the Kaoping River basin had average velocities ranging from 20.9 m/s to 50.6 m/s thus indicating that the movement velocities of the landslides in Linpien River and Taimali River basins were faster than those in the Kaoping River basin. In addition, the average gradient of the landslide slopes in the Linpien River basin and Taimali River basin, approximately 22°, were steeper than those of 18° in the Kaoping River basin. The positive relationship between the slope gradients and movement velocities for these events corroborates intuition, demonstrating that landslides on steeper slopes move faster (Fig. 5). However, although the slope gradients of L01, K01 and K04 were less than 20°, their movement velocities still exceeded 50 m/s, which implied that the movement velocity of landslides would not be influenced solely by slope gradient, but also by friction.

The landslides described in this study demonstrated reasonably large velocities in comparison to previous research, but are reasonable for the study environment. For example, Lo et al. (2014) applied a friction coefficient of 0.1 in their simulation using PFC3D for Hsiaolin landslide (K02 in the study), estimating a duration of 112 s, yielding an average speed of 26.79 m/s, slightly less than the velocity, 32.3 m/s, estimated from seismic signals. In addition, Tsou et al. (2011) reported that the velocities of K02 landslide ranged from 20.4 m/s to 33.7 m/s, roughly equivalent to the results of this

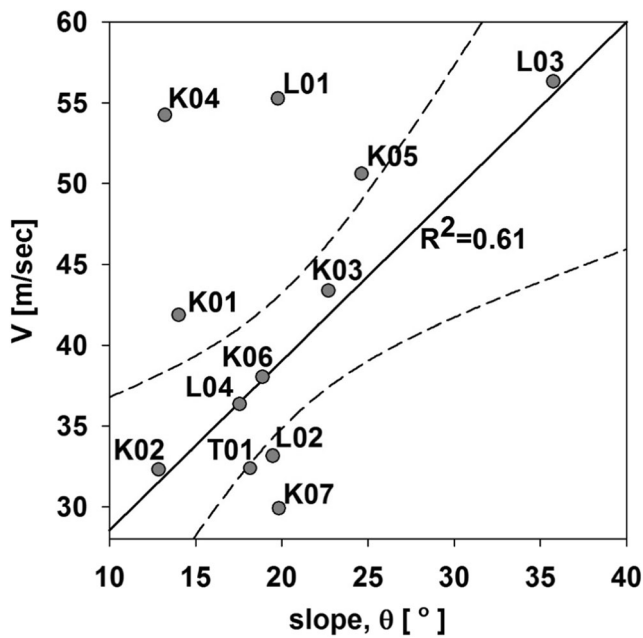
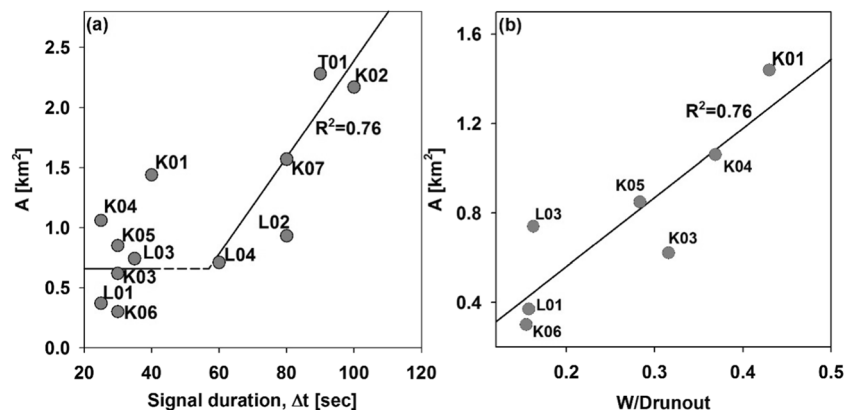


Fig. 5 Slope gradient versus landslide velocity. The solid lines indicate linear regression fits and the dashed lines mean 95% confidence interval

case study. Kuo et al. (2011) conducted a computer simulation for K02 landslide, and they considered that the average velocities ranged from 35 m/s to 40 m/s with a maximum of 50 m/s. The study of Lin (2015) reported that an average velocity of K02 landslide was 53 m/s, which was even larger than the average velocity estimated in the study. Many of these calculations are significantly affected by inferred friction of the landslide mass during movement—further discussion of the sensitivity of landslide velocity to friction is provided in the next section.

The correlation between disturbed areas and sliding duration was most pronounced when travel time (Δt) was greater than 60 s. For landslides with $\Delta t < 40$ s, there was no obvious relationship between disturbed area and signal duration (Fig. 6a). However, for events with $\Delta t > 40$ s, disturbed areas possessed a linear relationship ($R^2 = 0.76$) with the aspect ratio of landslide source width and runout distance (Fig. 6b).

Fig. 6 (a) Landslide signal duration versus disturbed area. (b) The ratio of width of landslide source area to runout distance (W/D_{runout}) versus disturbed area. The solid lines indicate linear regression fits



These results suggest that, for landslides with longer travel duration, disturbed areas tend to be more dependent by the duration of landslide movement, but for landslides with shorter duration, the disturbed areas tend to be more dependent on the geometric shapes of landslide source areas. It is important to highlight that the results presented herein are specific to certain terrain and triggering conditions, and the limited number of recorded events certainly does not provide universal insight into the runout behavior of all landslides. The empirical nature of these results, the complexity of triggering conditions, and the variability of site conditions worldwide would require different landslide travel relationships to be developed. However, the approach proposed herein may be a simple way to establish basic runout parameters. The results presented herein may also be useful for landslides that occur in similar terrain, geology and extreme climactic conditions.

Landslide travel duration and inferred physical properties

The runout behavior of landslides is often described in context of the law of conservation of energy (Scheidegger 1973; Terlien et al. 1995). Assuming that the totality of landslide debris acts as a single mass moving downslope on a single sliding surface and that the total energy of a sliding system remains constant over time, the conversion of potential energy, kinetic energy, and energy loss during sliding may be simplified and expressed as:

$$\Delta E_U = \Delta E_K + F \cdot S \tag{1}$$

where ΔE_U is the change of potential energy during mass movement, ΔE_K is the change of kinetic energy during mass movement, F is the friction during mass movement, and S is the runout distance of mass movement (D_{runout}). The changes of potential energy ΔE_U , kinetic energy ΔE_K , and friction F for a downward mass with zero initial velocity are defined as:

$$\Delta E_U = m \cdot g \cdot D_v \tag{2}$$

$$\Delta E_K = 0.5 \cdot m \cdot V^2 \tag{3}$$

$$F = \mu \cdot N \tag{4}$$

where m is the mass of the landslide, g is the acceleration due to gravity, D_v is the vertical displacement of landslide mass, V is the average quasi-front velocity of landslide mass, μ is the average friction coefficient, and N is the normal force of landslide mass. Hence, the formula of conservation of energy can be defined as:

$$m \cdot g \cdot D_{runout} \cdot \sin(\theta) = 0.5 \cdot m \cdot (D_{runout}/\Delta t)^2 + \mu \cdot m \cdot \cos(\theta) \cdot g \cdot D_{runout} \tag{5}$$

and simplified as:

$$D_{runout} = 2 \cdot g \cdot (\sin(\theta) - \mu \cdot \cos(\theta)) \cdot \Delta t^2 \tag{6}$$

Consequently, Eq. (6) implies that runout distance (D_{runout}) should have a positive correlation to the square of signal duration (Δt) and a negative correlation with the friction coefficient of the failing mass. The observed relationship between runout and travel duration for the 12 landslides is consistent with expected correlations between of observed square of signal durations and runout distances (Fig. 7), defined as $D_{runout} = 0.198\Delta t^2 + 1296$ m ($R^2 = 0.92$) for the given terrain. Knowing the slope of each landslide’s travel path, the linear relationship between D_{runout} and Δt^2 enables back-calculation of friction coefficients that are useful for future projected runout behavior. The mean friction coefficients calculated for the 12 landslides result in values of μ ranging from 0.12 to 0.62, with variability likely owing to estimates in slope, lack of subsurface conditions, and differences in lithology and geology between the Linpien River basin and Kaoping

River basin (Table 1). The calculated friction coefficients ranged between 0.12 and 0.36 for the sedimentary geology comprising the seven landslides in the Kaoping River basin, resulting in a mean friction coefficient of 0.26. In the Linpien River basin, calculated friction coefficients ranged from 0.24 to 0.62, with a mean μ of 0.30 for the metamorphic slates that comprised the four recorded landslides. Finally, the single massive landslide recorded in the Tamali River basins has a calculated friction coefficient of 0.36. While there is a range of friction coefficients, these back-calculated values tend to agree with the limited studies in the area. For example, using alternative methods, other studies have estimated the friction coefficient for K02 landslide ranging from 0.1 to 0.25 (Lo et al. 2014; Tsou et al. 2011). The average friction coefficient of 0.21 for the K02 landslide estimated in the study was consistent with these estimates. While friction coefficients are one of the most crucial parameters for determining the dynamic processes of a landslide runout, their direct measurement in the field remains difficult. These values estimated in the study represent the average friction coefficients, and they are useful in assessing runout hazard from large-scale precipitation-induced landslides in southern Taiwan.

Critical rainfall threshold for large landslide initiation

Estimates of landslide initiation time were made from ground motion records—this information was directly incorporated with measured rainfall records to gather insight into potential precipitation thresholds for large-scale landslide occurrence. In order to define the rainfall threshold for landslide initiation, a detailed analysis of the rainfall characteristics, i.e. rainfall duration D , intensity I and cumulative rainfall R , was performed against the 12 landslides considered in this case study. Rainfall thresholds were defined in terms of mean intensity (mm/h), and rainfall duration (h). For comparative purposes, an inventory of thirty-four small-scale landslides (<0.3 km²) and their respective initiation times and precipitation records were provided by the Soil and Water Conservation Bureau, Taiwan (Fig. 8a). One clear difference between the smaller landslide-rainfall thresholds and those for the 12 large slides is that the latter occurs primarily during longer rainfall durations and cumulative precipitation levels. However, the smaller slides are more likely for smaller, but intense precipitation events (Fig. 8b).

Caine (1980) collected the rainfall records of worldwide shallow landslides and defined a critical rainfall threshold in terms of rainfall intensity and duration. Since then, numerous rainfall thresholds proposed for various climatic and geological regions (Jibson 1989; Larsen and Simon 1993; Chen et al. 2005; Hong et al. 2005; Guzzetti et al. 2008; Saito et al. 2010). The general form of the threshold curves can be expressed in the following form (Caine 1980):

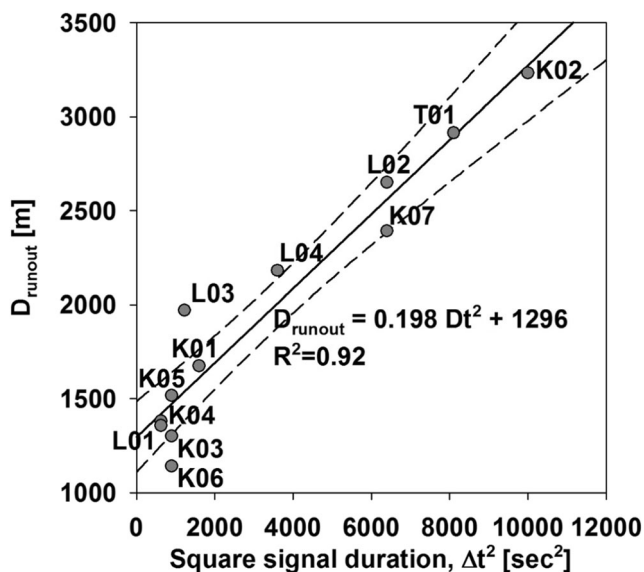
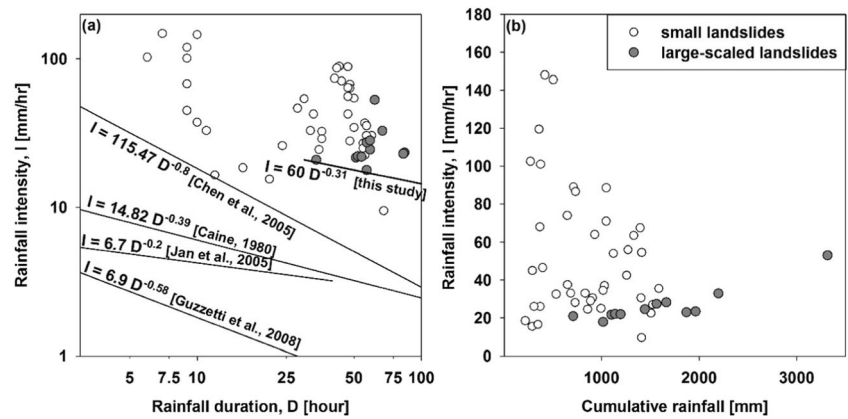


Fig. 7 Square signal duration versus runout distance. The solid lines indicate linear regression fits and the dashed lines mean 95% confidence interval

Fig. 8 Rainfall records at the time of landslide initiation. (a) Rainfall duration versus rainfall intensity. (b) Cumulative rainfall versus rainfall intensity. The solid circles show the 12 landslides as detected from seismic records, and the hollow circles indicate the 34 landslides investigated by the Soil and Water Conservation Bureau, Taiwan during 2005–2009



$$I = \alpha \times D^{-\beta} \tag{7}$$

where I is the rainfall intensity (mm/h), D is the duration of the rainfall event (h), α is the intercept, and β defines the slope of the power law curve. According to the rainfall measurements at the incipient time of failure for the 12 observed landslides, the rainfall threshold is defined in the range of duration D between 30 and 85 h may be expressed in the form:

$$I = 60 \times D^{-0.31} \tag{8}$$

A comparison of the rainfall thresholds for the 12 landslides (i.e. eq. 8) and other region- or geology-specific thresholds reported in the literature reveals that the threshold curves in the case study were significantly higher than those from Caine (1980), Chen et al. (2005), Jan and Chen (2005), and Guzzetti et al. (2008) (Fig. 8a). This is attributable to the specific nature of the slides studied; the landslides of interest were specifically large in area, and had significant runout distances. That is, significant rainfall may be necessary to mobilize landslides of this magnitude. Thus, it is desirable to have more extensive landslide inventories to enhance the reliability of rainfall thresholds for the large-scale landslide discussed herein; however, the propose threshold is a start to better quantifying hazards in southern Taiwan.

Limitations and future work

The disturbed areas in this case study, all exceeding 0.30 km², were 30 times larger than the mean slope failures (0.01 km²) that occurred during typhoon Morakot (Lin et al. 2011). This highlights that generally only larger slides were captured from ground motion records. The surface wave magnitudes, M_s , of the 12 landslides showed that the K03 landslide had the smallest M_s at 4.4 and the T01 landslide had the largest M_s at 5.4 (Table 1). The magnitudes of surface waves increased with greater landslide areas (Fig. 9). Among the 12 observed landslides, K02, K07 and T01 were the three largest by area,

and thus could be expected to have greater relative mass and maximum force during runout, possibly providing more confidence in the analysis of seismic records. Although large debris volumes and mass may produce more coherent ground motions, the lower limit of this mass threshold is still undetermined. In general, ground motion records consist of many different input sources, and the amplitude of ground motions decays with an increase in distance between the seismic station to the source of vibration (Weichert et al. 1994; Surinach et al. 2005; Ekstrom and Stark 2013). Therefore, ground motions induced by small-scale landslides are difficult to isolate and current application of seismic inversions for landslide detection remain constrained to large-scale landslides. However, more refined and sensitive techniques that may infer smaller slope failures would significantly improve assessment of landslide hazards, particularly considering specific regional geology or climactic conditions.

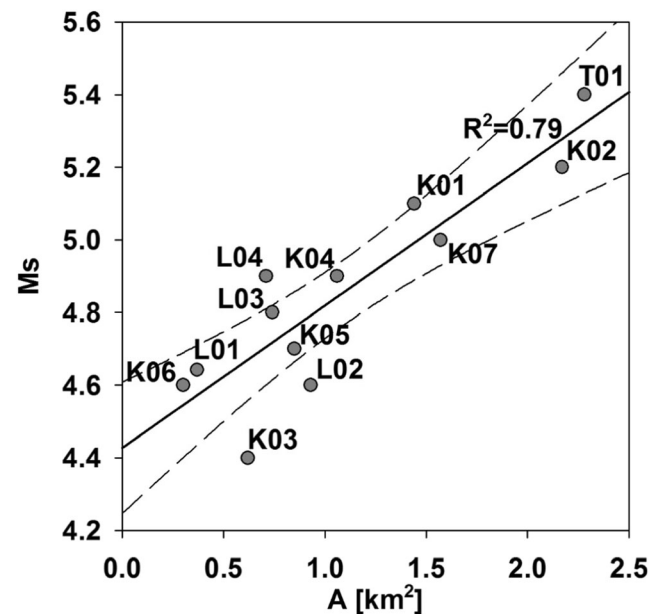


Fig. 9 Disturbed area (A) versus calculated surface wave magnitude (M_s). The solid lines indicate linear regression fits and the dashed lines mean 95% confidence interval

Conclusions

This study highlights some of the findings associated with large-scale landslides in southern Taiwan that occurred as a result of Typhoon Morakot in 2009. After a cumulative rainfall in excess of 2000 mm, 12 large-scale landslides with areas in excess of 0.3 km² were detected and located from the record of seismic ground motions. Geomorphic changes and seismic records indicate that as the duration of the associated landslide movements exceeded 60 s, and the landslide-disturbed areas were positively correlated with landslide travel times. However, if the travel durations were under 40 s, the landslide-disturbed area correlated better with the geometric shape of the landslide source area. For the specific geologic and climactic conditions within this region, a positive relationship between the runout distance and the square of movement duration of landslides can be expressed through the formula $D_{runout} = 0.198 \cdot \Delta t^2 + 1296$. Assessments of the friction coefficients and associated runout distances of potential landslides can be carried out using the proposed Δt - D_{runout} relationship.

Records of the investigated ground motions provide accurate estimates of landslide initiation time. Such information enables the assessment of the critical rainfall thresholds outside of what is reported in the literature for other geologic or climactic regimes. The rainfall threshold for the 12 large-scale landslides detected by ground motions was defined in terms of rainfall intensity and duration as $I = 60 \cdot D^{-0.31}$. The rainfall threshold for the 12 observed landslides was higher than those for shallow or small-scale landslides. Generally, the results shown indicate that in this region, only ground motions resulting from large-scale landslides could be observed and extracted using seismic records.

Acknowledgements This work was generously supported by the Ministry of Science and Technology, Taiwan. The authors are grateful to Academic Sinica and Central Weather Bureau, Taiwan for providing seismic records of the broadband array of Taiwan system. We also would like to thank Aerial Survey Office, Forestry Bureau, Taiwan, which provided the remote sensing images and digital terrain model for this study.

References

- Brodsky EE, Gordeev E, Kanamori H (2003) Landslide basal friction as measured by seismic waves. *Geophys Res Lett* 30(24):2236. <https://doi.org/10.1029/2003GL018485>
- Burt CC (2007) *Extreme weather: a guide & record book*. W. W. Norton & Company, Inc, New York
- Caine N (1980) The rainfall intensity - duration control of shallow landslides and debris flows. *Geografiska Annaler: Ser A, Phys Geog* 62: 23–27. <https://doi.org/10.1080/04353676.1980.11879996>
- Central Geological Survey (2013) *Geological Investigation & Database Construction for upstream of flood prone area*. Central Geological Survey. MOEA, New Taipei City, Taiwan (in Chinese)
- Chao WA, Zhao L, Chen SC, Wu YM, Chen CH, Huang HH (2016) Seismology-based early identification of dam-formation landslide events. *Sci Rep* 6:19259. <https://doi.org/10.1038/srep19259>
- Chen CH, Chao WA, Wu YM, Zhao L, Chen YG, Ho WY, Lin TL, Kuo KH, Chang JM (2013) A seismological study of earthquakes using a real-time broad-band seismic network. *Geophys J Int* 194:885–898. <https://doi.org/10.1093/gji/ggt121>
- Chen CY, Chen TC, Yu FC, Yu WH, Tseng CC (2005) Rainfall duration and debris-flow initiated studies for real-time monitoring. *Environ Geol* 47:715–724. <https://doi.org/10.1007/s00254-004-1203-0>
- Chen H, Lin GW, Lu MH, Shih TY, Horng MJ, Wu SJ, Chuang B (2011) Effects of topography, lithology, rainfall and earthquake on landslide and sediment discharge in mountain catchments of southeastern Taiwan. *Geomorphology* 133:132–142. <https://doi.org/10.1016/j.geomorph.2010.12.031>
- Chen TC, Lin ML, Wang KL (2014) Landslide seismic signal recognition and mobility for an earthquake-induced rockslide in Tsaoling, Taiwan. *Eng Geol* 171:31–44. <https://doi.org/10.1016/j.enggeo.2013.11.018>
- Cruden DM, Varnes DJ (1996) Landslide types and processes. In: Turner AK, Schuster RL (eds) *Special report 247: landslides investigation and mitigation*. National Academy Press, Washington D.C., p 673
- CWB (2013) *Report on typhoons in 2009*. Central Weather Bureau, Taipei (In Chinese)
- Dammeier F, Moore JR, Haslinger F, Loew S (2011) Characterization of alpine rockslides using statistical analysis of seismic signals. *J Geophys Res* 116:F04024. <https://doi.org/10.1029/2011JF002037>
- Ekstrom G, Stark CP (2013) Simple scaling of catastrophic landslide dynamics. *Science* 339:1416–1419. <https://doi.org/10.1126/science.1232887>
- Feng Z (2011) The seismic signatures of the 2009 Shialin landslide in Taiwan. *Nat Hazard Earth Sys* 11:1559–1569. <https://doi.org/10.5194/nhess-11-1559-2011>
- Feng ZY (2012) The seismic signatures of the surge wave from the 2009 Xiaolin landslide-dam breach in Taiwan. *Hydrol Process* 26:1342–1351. <https://doi.org/10.1002/hyp.8239>
- Guzzetti F, Peruccacci S, Rossi M, Stark CP (2008) The rainfall intensity-duration control of shallow landslides and debris flows: an update. *Landslides* 5:3–17. <https://doi.org/10.1007/s10346-007-0112-1>
- Hibert C, Ekström G, Stark CP (2014) Dynamics of the Bingham canyon mine landslides from seismic signal analysis. *Geophys Res Lett* 41(13):4535–4541
- Ho CS (1994) *An introduction to the geology of Taiwan explanatory text of the geologic map of Taiwan*. Central Geological Survey, Taipei. (in Chinese)
- Hong Y, Hiura H, Shino K, Sassa K, Suemine A, Fukuoka H, Wang GH (2005) The influence of intense rainfall on the activity of large-scale crystalline schist landslides in Shikoku Island, Japan. *Landslides* 2: 97–105. <https://doi.org/10.1007/s10346-004-0043-z>
- Hung C, Lin GW, Syu HS, Chen CW, Yen HY (2017) Analysis of the Aso-bridge landslide during the 2016 Kumamoto earthquakes in Japan. *J Bull Eng Geol Environ*. <https://doi.org/10.1007/s10064-017-1103-7>
- Hung C, Liu CH, Lin GW, Leshchinsky B (2018) The Aso-bridge coseismic landslide: a numerical investigation using finite and discrete element methods. *Bull Eng Geol Environ*. <https://doi.org/10.1007/s10064-018-1309-3>
- IES (1996) *Broadband Array in Taiwan for seismology*. Institute of Earth Sciences, Academia Sinica, Taiwan. Other/Seismic Network. <https://doi.org/10.7914/SN/TW>
- Jan CD, Chen CL (2005) Debris flows caused by typhoon herb in Taiwan. In: Jakob M, Hung O (eds) *Debris flow hazards and related phenomena*. Springer, New York, pp 539–563
- Jibson RW (1989) Debris flows in southern Puerto Rico. *Geol Soc Am Spec Pap* 236:29–55. <https://doi.org/10.1130/SPE236-p29>

- Jaboyedoff M, Oppikofer T, Abellán A, Derron MH, Loye A, Metzger R, Pedrazzini A (2012) Use of LIDAR in landslide investigations: a review. *Nat Hazards* 61(1):5–28. <https://doi.org/10.1007/s11069-010-9634-2>
- Kanamori H, Given JW (1982) Use of long-period surface-waves for rapid-determination of earthquake source parameters. *Phys Earth Planet Inter* 30:260–268. [https://doi.org/10.1016/0031-9201\(81\)90083-2](https://doi.org/10.1016/0031-9201(81)90083-2)
- Kao H, Kan CW, Chen RY, Chang CH, Rosenberger A, Shin TC, Leu PL, Kuo KW, Liang WT (2012) Locating, monitoring, and characterizing typhoon-induced landslides with real-time seismic signals. *Landslides* 9:557–563. <https://doi.org/10.1007/s10346-012-0322-z>
- Kawakatsu H (1989) Centroid single force inversion of seismic waves generated by landslides. *J Geophys Res: Solid Earth* 94(B9):12363–12374. <https://doi.org/10.1029/JB094iB09p12363>
- Kimura H, Yamaguchi Y (2000) Detection of landslide areas using satellite radar interferometry. *Photogramm Eng Remote Sens* 66(3):337–344
- Kuo, CY, Tai, YC, Chen, CC, Chang, KJ, Siau, AY, Dong, JJ, Han, RH, Shimamoto T, Lee CT (2011) The landslide stage of the HsiaoLin catastrophe: simulation and validation. *J Geophys Res* 116:F04007. <https://doi.org/10.1029/2010JF001921>
- Kuo YS, Tsai YJ, Chen YS, Shieh CL, Miyamoto K, Itoh T (2013) Movement of deep-seated rainfall-induced landslide at HsiaoLin Village during typhoon Morakot. *Landslides* 10:191–202. <https://doi.org/10.1007/s10346-012-0315-y>
- Larsen MC, Simon A (1993) A rainfall intensity-duration threshold for landslides in a humid-tropical environment, Puerto-Rico. *Geogr Ann A* 75:13–23. <https://doi.org/10.1080/04353676.1993.11880379>
- Lin CH, Kumagai H, Ando M, Shin TC (2010) Detection of landslides and submarine slumps using broadband seismic networks. *Geophys Res Lett* 37:L22309. <https://doi.org/10.1029/2010GL044685>
- Lin CH (2015) Insight into landslide kinematics from a broadband seismic network. *Earth, Planets Space* 67:8. <https://doi.org/10.1186/s40623-014-0177-8>
- Lin CH, Jan JC, Pu HC, Tu Y, Chen CC, Wu YM (2015) Landslide seismic magnitude. *Earth Planet Sci Lett* 429:122–127. <https://doi.org/10.1016/j.epsl.2015.07.068>
- Lin CW, Chang WS, Liu SH, Tsai TT, Lee SP, Tsang YC, Shieh CL, Tseng CM (2011) Landslides triggered by the 7 august 2009 typhoon Morakot in southern Taiwan. *Eng Geol* 123:3–12. <https://doi.org/10.1016/j.enggeo.2011.06.007>
- Lin GW, Hung C, Syu HS (2017) Evaluation of an enhanced FS method for finding the initiation time of earthquake-induced landslides. *Bull Eng Geol Environ*. <https://doi.org/10.1007/s10064-017-1083-7>
- Lo CM, Lee CF, Chou HT, Lin ML (2014) Landslide at Su-Hua highway 115.9k triggered by typhoon Megi in Taiwan. *Landslides* 11(2):293–304
- Nichol J, Wong MS (2005) Satellite remote sensing for detailed landslide inventories using change detection and image fusion. *Int J Remote Sens* 26(9):1913–1926. <https://doi.org/10.1080/01431160512331314047>
- Saito H, Nakayama D, Matsuyama H (2010) Relationship between the initiation of a shallow landslide and rainfall intensity-duration thresholds in Japan. *Geomorphology* 118:167–175. <https://doi.org/10.1016/j.geomorph.2009.12.016>
- Shieh SL (2000) Users' guide for typhoon forecasting in the Taiwan area (VIII). Central Weather Bureau, Taipei
- Surinach E, Vilajosana I, Khazaradze G, Biescas B, Furdada G, Vilaplana JM (2005) Seismic detection and characterization of landslides and other mass movements. *Nat Hazard Earth Sys* 5:791–798. <https://doi.org/10.5194/nhess-5-791-2005>
- Scheidegger AE (1973) On the prediction of the reach and velocity of catastrophic landslides. *Rock Mech* 5:231–236. <https://doi.org/10.1007/BF01301796>
- Terlien MTJ, Van Westen CJ, van Asch TWJ (1995) Deterministic modeling in Gis-based landslide Hazard assessment. In: Carrara A, Guzzetti F (eds) *Geographical information systems in assessing natural hazards. advances in natural and technological hazards research*, vol 5. Springer, Dordrecht. https://doi.org/10.1007/978-94-015-8404-3_4
- Tsou CY, Feng ZY, Chigira M (2011) Catastrophic landslide induced by typhoon Morakot, ShiaoLin, Taiwan. *Geomorphology* 127:166–178. <https://doi.org/10.1016/j.geomorph.2010.12.013>
- Varnes DJ (1978) Slope movement types and processes. In: Schuster RL, Krizek RJ (eds) *Special report 247: landslides, analysis and control*. National Academy of Sciences, Washington D.C., p 234
- Weichert D, Homer RB, Evans SG (1994) Seismic signatures of landslides: the 1990 Brenda mine collapse and the 1965 Hope rockslides. *B Seismol Soc Am* 84(5):1523–1532
- Wu CH, Chen SC, Chou HT (2011) Geomorphologic characteristics of catastrophic landslides during typhoon Morakot in the Kaoping watershed, Taiwan. *Eng Geol* 123:13–21. <https://doi.org/10.1016/j.enggeo.2011.04.018>